Soft Matter

PAPER

View Article Online
View Journal | View Issue



Cite this: *Soft Matter*, 2021, **17**, 4161

# Constitutive modeling of strain-dependent bond breaking and healing kinetics of chemical polyampholyte (PA) gel†

Sairam Pamulaparthi Venkata, ‡[a] Kunpeng Cui, ‡[b] Jingyi Guo,[a] Alan T. Zehnder,[a] Jian Ping Gong [bcd] and Chung-Yuen Hui *[ac]

Received 21st January 2021,
Accepted 26th February 2021

DOI: 10.1039/d1sm00110h

rsc.li/soft-matter-journal

A finite strain nonlinear viscoelastic constitutive model is used to study the uniaxial tension behaviour of chemical polyampholyte (PA) gel. This PA gel is cross-linked by chemical and physical bonds. Our constitutive model attempts to capture the time and strain dependent breaking and healing kinetics of physical bonds. We compare model prediction by uniaxial tension, cyclic and relaxation tests. Material parameters in our model are obtained by least squares optimization. These parameters gave fits that are in good agreement with the experiments.



## 1. Introduction

Hydrogels are soft and wet materials often occurring in nature as biotissues.[1] Hydrogels are composed of a polymer network swollen by water. These features make hydrogels well suited for many bio-engineering applications, such as cell scaffolds in tissue engineering,[2–4] as artificial cartilage,[5,6] and as vehicles for drug delivery.[7–9] Conventional hydrogels are mechanically soft and weak,[10] which severely limits their applications, especially in structural biomaterials.[10] The pioneering work of double network hydrogels (DN gels) by Gong *et al.*[11] improved the mechanical strength and toughness of hydrogels.[12,13] DN gels are composed of a stiff/brittle first network and a soft/stretchable second network. During deformation, the first network breaks preferentially to dissipate energy, while the second network keeps the sample intact. DN gels have a high toughness of $\sim$1000 J m$^{-2}$, which is comparable to the cartilage.[14]

Studies on DN gels revealed a general strategy to toughen network materials. That is, incorporating a sacrificial structure into the polymer network to dissipate mechanical energy.[10] Along this line, many strong and tough hydrogels have been developed in recent years.[15–21] Among them, the hydrogels with physical bonds as sacrificial structures are especially interesting. Diverse physical bonds have been used to toughen hydrogels, including metal–ion interaction,[15] hydrogen bonding,[22–24] ionic interaction,[25,26] host–guest interaction,[27,28] π–π stacking,[29] and so on.[30,31] Physical bonds are dynamic and reversible; thus, they not only improve the toughness, but also endow the gels with time- or rate-dependent mechanical behaviour, together with self-recovery and self-healing abilities.[25] As the dissociation and association of physical bonds fundamentally govern the mechanical properties,[32] it is important to understand the bond kinetics of these gels.

In a recent work, we developed a generalized constitutive model to quantitatively understand the bond kinetics of a purely physically cross-linked hydrogels composed of polyampholytes (PA gels).[33] PA gels are synthesized by random copolymerization of cationic and anionic monomers at high concentrations around the charge balanced point.[25,34] As a result, PA chains carry almost the same number of opposite charges on average, and the charges are randomly distributed on the chain backbones. PA gels exhibit a combination of mechanical performance, such as high toughness, high stiffness, high fatigue resistance, high viscoelasticity, self-recovery, and self-healing.[25,35–37] Pure physical PA gels, *i.e.* PA gels without a chemical cross-linker, have a phase-separated structure, with a polymer rich phase and a polymer poor phase.[38–40] Due to this phase separation, we used two types of bond kinetics to capture the time-dependent mechanical behaviour of these pure physical hydrogels.[33] For PA gels with a chemical cross-linker (greater than 1 mol% relative to the total monomer concentration), which are referred as chemical PA gels here, the gels become homogeneous and we observe no phase

[a] *Field of Theoretical and Applied Mechanics, Department of Mechanical and Aerospace Engineering, Cornell University, Ithaca, New York, 14853, USA. E-mail: ch45@cornell.edu*
[b] *Institute for Chemical Reaction Design and Discovery (WPI-ICReDD), Hokkaido University, Sapporo 001-0021, Japan*
[c] *Soft Matter GI-CoRE, Hokkaido University, Sapporo 001-0021, Japan*
[d] *Faculty of Advanced Life Science, Hokkaido University, Sapporo 001-0021, Japan*

† Electronic supplementary information (ESI) available. See DOI: 10.1039/d1sm00110h

‡ These authors contributed equally to this work. Numerical simulations are performed by Sairam Pamulaparthi Venkata. Experimental data is provided by Kunpeng Cui.

separation.[40] These gels show very different mechanical behaviour compared with pure physical hydrogels. For example, the fracture strain of pure physical PA hydrogels increases as the loading rate decreases, while the fracture strain of chemical PA gels is insensitive to the loading rate. In addition, these chemical gels fail in a tension test at much lower strains. It is therefore interesting to see whether our previous theory can be used to predict the mechanical behaviour of this PA gel. For this purpose, we use one type of bond kinetics for all the physical cross-links and put into the role of a chemical crosslinker, as this PA gel is chemically cross-linked and has a homogeneous structure. We found that the modified theory works well in describing the time-dependent mechanical behaviour of chemical PA gels.

Our present work is structured in the following manner. In Section 2, we state the theoretical model and the nominal stress–strain relationship for different types of loading histories. In Section 3, we briefly describe an experimental procedure for the synthesis and mechanical testing of the chemical PA gel. In Section 4, we identify and discuss the material parameters required in our finite strain constitutive model. In Section 5, we validate the accuracy of our theory by comparing the simulation results with the experiments. We observe that our model predicts the experiments well. Conclusions are presented in Section 6.

## 2. Theory

In our previous works, we formulated a 3D finite strain viscoelastic model for polyvinyl alcohol (PVA) hydrogels consisting of physical and chemical cross-links.[32,41,42] The breaking kinetics of physical cross-links in a PVA gel is found to be independent of the applied strain. Although this is a good assumption for the PVA gel, we found that bond breaking kinetics in a physically cross-linked PA gel is strain dependent which is necessary to explain the mechanical behaviour for different loading histories.[33] As noted above, we used two types of bond kinetics to capture the time-dependent mechanical behaviour of pure physical hydrogels. In this current work, our chemical PA gel consists of both physical and chemical cross-links. These chemical crosslinks form a permanent network. Deformation of this permanent network is elastic and time independent. The idea is to modify our previous model[33] by replacing one type of physical crosslinks with permanent chemical crosslinks. By considering the stress contributions from chemical cross-links along with physical cross-links, we obtain the nominal stress $P(t)$ in a uniaxial tension test where the stretch history $\lambda(t)$ is prescribed. Since the derivation of the constitutive model is practically identical to our previous work,[33] we summarize the details in the ESI.† The nominal stress $P$ is defined as the tensile force divided by the cross-sectional area of the undeformed sample. The stretch or stretch ratio $\lambda$ is defined as the displacement divided by the gauge length of the undeformed sample. The strain rate is defined as the stretching speed divided by the gauge length of the undeformed sample. Here we provide physical explanations to the material parameters in the stress equation (eqn (1a)) to aid a better understanding.

The nominal stress $P$ is given by (see, ESI† Section S4 for detailed derivation)

$$\begin{aligned} P(t) &= 2\omega_{\text{chem}}\left.\frac{\mathrm{d}W_0}{\mathrm{d}I_1}\right|_{I_1(t)}\left(\lambda(t)-\lambda(t)^{-2}\right) \\ &\quad + 2\rho\left.\frac{\mathrm{d}W_0}{\mathrm{d}I_1}\right|_{I_1(t)}\left[\phi_{\text{B}}\left(\tau=0,t,H^{0\to t}\right)\right]^{2-\alpha_{\text{B}}}\left(\lambda(t)-\lambda(t)^{-2}\right) \\ &\quad + \int_0^t\left[\chi(\tau)\phi_{\text{B}}(\tau,t,H^{\tau\to t})2\left.\frac{\mathrm{d}W_0}{\mathrm{d}I_1}\right|_{I_1=H^{\tau\to t}}\left[\frac{\lambda(t)}{\lambda^2(t)}-\frac{\lambda(\tau)}{\lambda^2(t)}\right]\right]\mathrm{d}\tau, \end{aligned} \tag{1a}$$

where

$$\phi_{\text{B}}(\tau,t,H^{\tau\to t}) = \left[1+\frac{\alpha_{\text{B}}-1}{t_{\text{B}}}\int_\tau^t f(H^{\tau\to s})\mathrm{d}s\right]^{\frac{1}{1-\alpha_{\text{B}}}}. \tag{1b}$$

Eqn (1a) has three terms, here we explain the physics behind each term:

1. The first term in eqn (1a) is the stress carried by the chemical crosslinks, where $\omega_{\text{chem}}$ is the fraction of chemical crosslinks. In the constitutive model, chemical crosslinks are assumed to be permanent and do not break under mechanical loading. The strain energy density function for chemical and physical crosslinks is assumed to be the same and denoted by $W_0$. Since the gel is incompressible, we assume that $W_0$ depends only on the first invariant of the right Cauchy–Green tensor $I_1(t) = \text{trace}[(\mathbf{F}^{0\to t})^T(\mathbf{F}^{0\to t})]$, where $\mathbf{F}$ is the deformation gradient tensor. The superscript $0 \to t$ in the deformation gradient tensor $\mathbf{F}^{0\to t}$ indicates that it is measured from the reference configuration at $t = 0$ when the gel is undeformed. In uniaxial loading, $I_1(t) = \lambda^2(t) + \frac{2}{\lambda(t)}$, where $\lambda$ is the stretch ratio in the tensile test. The first term indicates that the network formed by chemical crosslinks is elastic, since the stress depends only on the current stretch. This term was absent in our previous work[33] due to the absence of chemical crosslinks.

2. Unlike chemical cross-links, crosslinks formed from physical bonds can break and heal. We assume before loading ($t < 0$) that the physical crosslinks have reached a state of dynamic equilibrium in which the healing rate is equal to the breaking rate; this steady state healing rate is denoted by $\chi^{\text{ss}}$. The function $\phi_{\text{B}}(\tau,t,H^{\tau\to t})$ in eqn (1a) is the survivability function, it is the fraction of physical cross-links that survive from the time of their formation $\tau$ to the current time $t$ (in the 2nd term of eqn (1a), $\tau = 0$ and $H^{\tau\to t} \equiv H^{0\to t} = I_1(t)$). The notation $H^{\tau\to t} \equiv H(\tau,t) \equiv \text{trace}[(\mathbf{F}^{\tau\to t})^T\mathbf{F}^{\tau\to t}]$. The reason for this notation is as follows: we assume that when a physical cross-link breaks, it loses all its strain energy, and when it is reattached at time $\tau$, it carries no strain energy at that time. This means that these crosslinks can only feel the deformation at the time of their birth. Thus, the deformation of chains connected by these cross-links is described using the deformed configuration at time $\tau$ as the reference configuration. With this understanding,

 

let us consider the third term in eqn (1a) before discussing the second term: the third term represents the stress carried by physical cross-links that break and reattach during the loading history. To understand this, we first note that because bond breaking depends on deformation, the healing rate and the breaking rate are no longer the same once loading starts. We denote the healing rate at the current time by $\chi(t)$. In our model, the healing rate is equal to the fraction of broken physical bonds divided by the characteristic healing time $t_H$ (for a physical motivation, see the ESI,† Section S1). Thus, the term $\chi(\tau)\phi_B(\tau,t,H^{\tau\to t})d\tau$ in the integral represents the fraction of bonds that reattach at time $\tau$ and survive to the current time $t$, and the stress they carry is $2\frac{dW_0}{dI_1}\Big|_{I_1=H^{\tau\to t}}\left[\frac{\lambda(t)}{\lambda^2(\tau)}-\frac{\lambda(\tau)}{\lambda^2(t)}\right]$. Thus, the integral is the stress carried by reattached bonds from the time of loading to the current time.

The function $\chi(t)$ depends on the loading history and is obtained by solving the following integral equation (eqn (2))[33]

$$\underbrace{\omega_{phys}}_{\text{Total fraction of physical bonds}} = 1-\omega_{chem} = \underbrace{\chi(t)t_H}_{\text{Fraction of broken physical bonds}} + \underbrace{\int_{-\infty}^{t}\phi_B(\tau,t,H^{\tau\to t})\chi(\tau)d\tau}_{\text{Fraction of connected physical bonds}} \quad (2)$$

3. Finally, let us consider the 2nd term in eqn (1a). The fraction of connected physical cross-links (number of connected physical cross-links over the total number of physical and chemical cross-links) before the start of loading is denoted by $\rho$. Therefore, the second term in eqn (1a) is the stress carried by the physical cross-links that remain connected from the start of loading ($\tau = 0$) to the current time $t$. Using the second term in the R.H.S. of eqn (2), $\rho$ is found to be (also see the ESI,† Section S2)

$$\rho = \frac{\chi^{ss}t_B}{2-\alpha_B}, \quad (3a)$$

$$\chi^{ss} = \frac{1-\omega_{chem}}{t_H+\frac{t_B}{2-\alpha_B}} \quad (3b)$$

Finally, we assume that the form of the survivability function is given by eqn (1b). In eqn (1b), $t_B$ is the characteristic breaking time of physical crosslinks, $\alpha_B \in (1, 2)$ is a material parameter that controls the rate of decay of the survivability function and $f$ is a function which measures the dependence of the breaking rate on the stretch experienced by a physical cross-link from its formation at time $\tau$ to the current time $t > \tau$. The physical motivation behind eqn (1b) can be found in the ESI† (Section S1).

In the following, we shall use eqn (1a) and (1b) to compute the nominal stresses during cyclic and relaxation tests. In these tests, the stretch ratio is given as a function of time. For example, in a perfect relaxation test, the stretch ratio is increased suddenly (at $t = 0^+$) to a value $\lambda_0 > 1$ and then held constant thereafter. For this case, the third term in eqn (1a) vanishes identically, indicating that the healing bonds do not carry any load in a perfect relaxation test. The nominal stress $P(t)$ relaxes according to:

$$P(t) = 2\left(\lambda_0-\lambda_0^{-2}\right)\frac{dW_0}{dI_1}\Big|_{I_1(\lambda_0)}\left\{\omega_{chem}+\rho\left[1+\frac{\alpha_B-1}{t_B}f(I_1(\lambda_0))t\right]^{\frac{2-\alpha_B}{1-\alpha_B}}\right\}. \quad (4)$$

In a real test, it is not possible to impose infinite strain rate, so eqn (4) needs to be modified to account for finite loading rate, and this modification is given in the ESI† (Section S4.2).

We end this section by stating an explicit form of the breaking function and the strain energy density function. The accelerating breaking function $f$ is given by

$$f(I_1) = \left(1+\frac{I_1-3}{I_c-3}\right)^m, \quad I_c = \lambda_c^2+\frac{2}{\lambda_c}, \quad (5)$$

where $\lambda_c$ is a characteristic stretch at which the breaking rate of physical crosslinks increases rapidly and $m$ is a material parameter controlling the breaking rate. For small strains, $\frac{I_1-3}{I_c-3} \ll 1$, $H^{\tau\to t} \approx 3$ and $f \approx 1$. Thus, in the small strain regime, the bond breaking kinetics is independent of strain, however, for larger strains, that is, when $I_1 - 3 > I_c - 3$, the breaking function $f$ increases rapidly. Further discussion of the physics behind the breaking function and critical strain is given in Sections S1 and S5.2 (see, ESI†) respectively. Different forms of strain energy function have been used in our previous works to account for strain hardening effects.[32,41,42] In the most recent work, $W_0(I_1)$ is given by Yeoh's model,[33] *i.e.*,

$$W_0(I_1) = \sum_{i=1}^{3} c_i(I_1-3)^i. \quad (6)$$

In Yeoh's model, $c_1 = \mu/2$ where $\mu$ is the small strain shear modulus of the undamaged network. The material parameters $c_2$ and $c_3$ control the strain hardening behaviour.

# 3. Experiments

## 3.1. Gel sample preparation

The procedure to prepare the chemical PA hydrogels was described in detail in our previous work.[38] Briefly, anionic monomer *p*-styrenesulfonate (NaSS), cationic monomer 3-(methacryloylamino)-propyl-trimethylammonium chloride (MPTC), photoinitiator α-ketoglutaric acid (α-keto), and chemical cross-linker *N*,*N*-methylene-bis-acrylamide (MBAA) were mixed to form an aqueous solution followed by UV polymerization. The obtained gels were immersed into a large amount of water for longer than one week to remove unreacted chemicals and counterions. The total monomer concentration, $C_m$, was 2.1 M, and the molar ratio of NaSS/MPTC was 0.525 : 0.475. The concentrations of MBAA and α-keto were 3 and 0.25 mol%, respectively, relative to $C_m$.

## 3.2. Mechanical testing

The procedures for mechanical testing are basically the same as that in our previous study.[33] In brief, we performed four sets of mechanical testing: uniaxial tensile test, small strain tensile

cyclic test, large strain tensile cyclic test, and tensile relaxation test. Gel samples for mechanical testing were cut into a dumbbell-like shape with the JIS K 6261-7 standard. The gauge length, width and thickness of the samples were 12, 2 and 1.74 mm, respectively. The samples were loaded in tension using a Shimadzu autograph machine with a 100 N load cell. The measurement was conducted in a water vapor environment to prevent gel dehydration.

## 4. Material parameters and their determination

The chemical PA gel constitutive model has 9 unknown independent material parameters in total. They are listed as follows: $\alpha_B$, $t_B$, $t_H$, $\omega_{phys}$ or $\omega_{chem}$, $m$, $\lambda_c$, $c_1 \equiv \mu/2$, $c_2$ and $c_3$. Once these 9 parameters are known, $\rho$ and $\chi^{ss}$ can be determined using eqn (3a) and (3b).

Some of these material parameters can be estimated from uniaxial tension and tensile-relaxation experimental data. For example, an estimate of the small strain instantaneous shear modulus ($\equiv\mu(\omega_{chem} + \rho) \approx 3.30$ MPa) can be found from the initial loading part of the tensile-relaxation test (see ESI,† Section S5.1). Similarly, an estimate of critical stretch ratio value, $\lambda_c \approx 1.20$ can be determined from the uniaxial tension data (see ESI,† Section S5.2). These estimates help us in selecting an optimal parameter set amongst multiple local optimums obtained from the least squares optimization process discussed in the ESI† (Section S6).

We use selected data from simple tension, tensile-relaxation, and cyclic tests and a least squares error optimization scheme to determine the 9 parameters. Since the same least squares optimization procedure was used to determine parameters in our recent work,[33] we have given the details of this procedure in the ESI† (Section S6). All the experimental data (see ESI,† Fig S3) except for one case (cyclic test with loading rate, LR and unloading rate, UR – 0.0014 $s^{-1}$ and 0.14 $s^{-1}$) were used in the optimization scheme to capture the material parameters mentioned in Table 1.

The material parameters obtained from the optimization process are summarized in Table 1. Table 1 shows that the characteristic breaking time of physical bonds is about ten times the healing time. Also, we note that the fraction of physical bonds connected before the start of loading ($\rho$) is just slightly lower than the total fraction of physical bonds ($\omega_{phys}$). This tells us that most of the physical cross-links are connected in the beginning of the test.

Our material parameters from the optimization scheme can predict reasonably well the loading history case which is not used in optimization process. The example being the cyclic test with LR (0.0014 $s^{-1}$) and UR (0.0014 $s^{-1}$). We observe that our material parameters simulate this loading history well. More importantly, if we use less experimental data in our optimization scheme – for example, by choosing alternative stretch ratio cases instead of all the stretch ratios in tensile-relaxation tests or by choosing alternative loading rate cases in cyclic tests or in simple tension tests, the optimized material parameters will fit all the experimental data well including the ones which we skipped in the optimization process, with less than 10% error between simulations and experiments.

## 5. Results

We compare our simulation results with simple tension, tensile-relaxation, and cyclic loading experimental data. These are shown in the following sections. It should be noted that simulations for all the different tests use the same material parameters from Table 1. Specifically, we solve eqn (1a) and (2) using the parameters in Table 1 to determine nominal stress and healing rates $\chi(t)$ respectively.

### 5.1. Nominal stress: cyclic tests (small strains)

The uniaxial cyclic tests for LR and UR of 0.014 $s^{-1}$ each in Fig. 1a and of 0.0014 $s^{-1}$ each in Fig. 1b for a small strain of 10% are shown in Fig. 1. This figure shows that our model slightly overestimates the experimental data for both cases.

Table 1 The material parameters required for constitutive model are listed below

| | | | |
|---|---|---|---|
| Strain dependent parameters | | | |
| $\alpha_B = 1.8001$ | $t_B = 0.1136$ s | $t_H = 0.01$ s | $\omega_{phys} = 0.99$ |
| Strain dependent accelerated breaking function parameters, $f$ | | | |
| $m = 4.8221$ | | | $\lambda_c = 1.2745$ |
| Undamaged network strain energy density function, Yeoh's model, $W_0$ | | | |
| $c_1 \equiv \mu/2 = 1.7911$ MPa | | $c_2/c_1 = 0.9703$ | $c_3/c_1 = 0.0245$ |
| Derived material parameters | | | |
| $\rho = 0.9729$ (see eqn (3a)) | $\chi^{ss} = 1.7117$ $s^{-1}$ (see eqn (3b)) | | $\mu(\omega_{chem} + \rho) \equiv \frac{E_0}{3} = 3.5210$ MPa |

Note that the small strain instantaneous shear modulus ($\mu(\omega_{chem} + \rho)$) and critical stretch ratio ($\lambda_c$) from Table 1 are consistent with those estimates given in the ESI (Section S5).

 

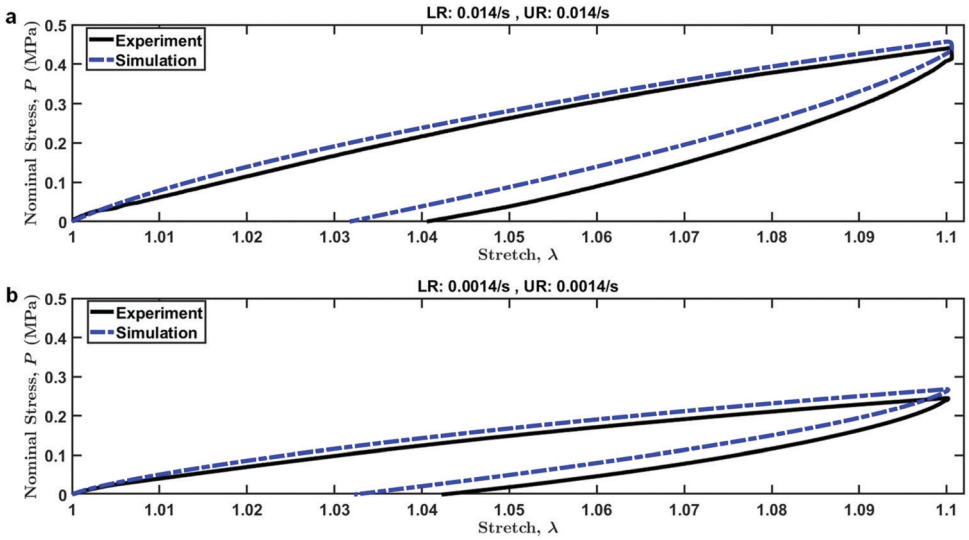


Fig. 1 Nominal stress $P$ (MPa) *vs.* stretch $\lambda$ for loading and unloading tests with two different strain rates are shown. (a) Loading rate (LR) and unloading rate (UR) of 0.014 $s^{-1}$ each. (b) LR and UR of 0.0014 $s^{-1}$ each. Solid black lines represent the experiment data and our simulation results using parameters in Table 1 are shown as dash-dotted blue lines.

**5.1.1. Large strain.** In Fig. 2 we compare the experimental data with our model prediction for cyclic tests with different LR and UR in the large strain regime. Fig. 2 shows that our model captures the experimental data well for all cases.

### 5.2. Tensile-relaxation tests

We compare our model with 6 different relaxation tests carried out with different stretch ratios $\lambda_0$ (Fig. 3).

Again, our model is in good agreement with experimental data in both the loading and the relaxation phases for all cases.

### 5.3. Simple tension

Simple tension tests with 6 different loading rates ranging over two decades are presented in Fig. 4. Our model predicts the experimental data for loading rates of 0.069 $s^{-1}$ and 0.14 $s^{-1}$ cases well. For the loading rate of 0.0014–0.014 $s^{-1}$, we observe an overestimation of nominal stress at higher stretch ratios after 2,

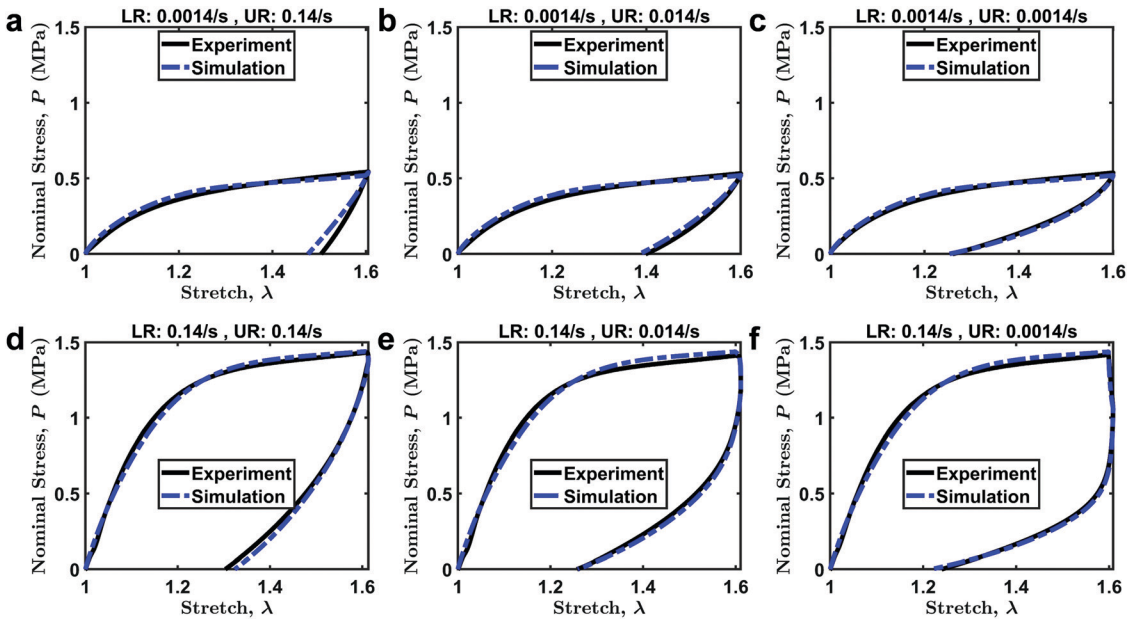


Fig. 2 Nominal stress $P$ (MPa) *vs.* stretch $\lambda$ for loading and unloading tests with different strain rates are shown here. (a–c) The upper plots have a loading rate (LR) of 0.14 $s^{-1}$ and unloading rates (UR) of 0.14 $s^{-1}$, 0.014 $s^{-1}$, and 0.0014 $s^{-1}$ from left to right respectively. (d–f) Similarly, the lower plots have a loading rate of 0.0014 $s^{-1}$ and unloading rates of 0.14 $s^{-1}$, 0.014 $s^{-1}$, and 0.0014 $s^{-1}$ from left to right respectively. Solid black lines represent the experiment data and our simulation results using parameters in Table 1 are shown as dash-dotted blue lines.

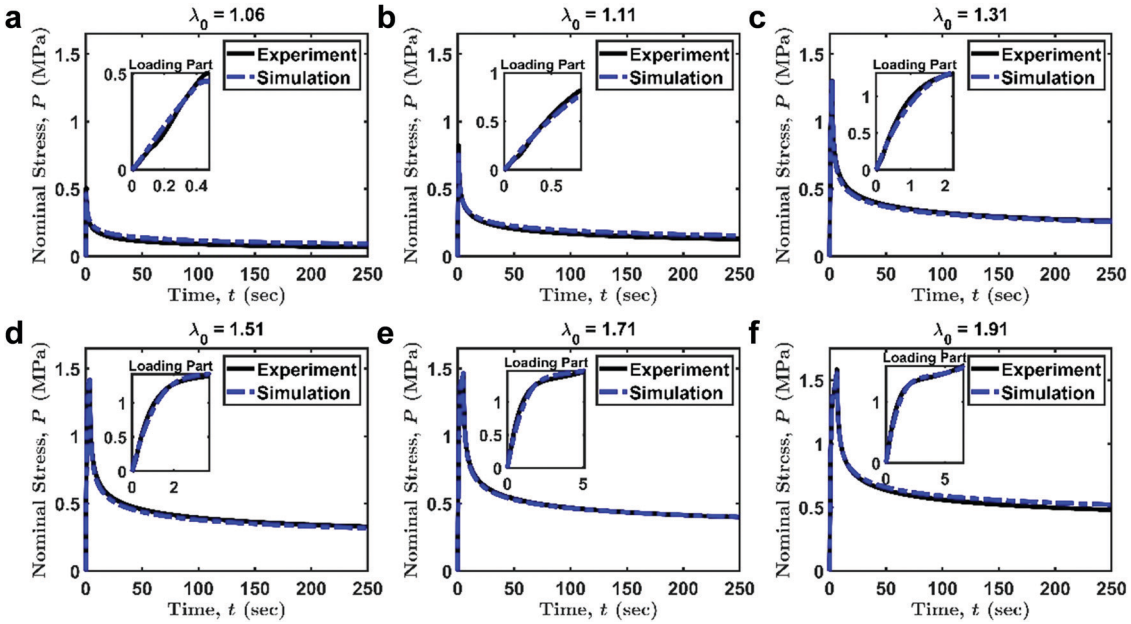


Fig. 3 Nominal stress $P$ (MPa) *vs.* time $t$ (sec) for tensile-relaxation tests with different nominal stretch ratios are shown here. Solid black lines represent the experiment data and our simulation results using parameters in Table 1 are shown as dash-dotted blue lines. Loading part of the tests are shown as insets. Relaxation tests are carried out at six stretch ratios (a) $\lambda_0$ = 1.06, (b) $\lambda_0$ = 1.11, (c) $\lambda_0$ = 1.31, (d) $\lambda_0$ = 1.51, (e) $\lambda_0$ = 1.71, and (f) $\lambda_0$ = 1.91.

as the model tends to harden more than the experimental data at slower loading rates. Similarly, at a higher loading rate of 0.68 $s^{-1}$, experiment is slightly overestimated by our model. On an average, the relative error between theory and experiment is less than 10% except for the lowest loading rate case of 0.0014 $s^{-1}$ at higher stretch ratios.

### 5.4. Load bearing characteristics of physical and chemical crosslinks, healing rate

The stress carried by physical and chemical bonds for different loading histories are shown in Fig. 5. To present a general trend, we select one case each from simple tension, tensile-relaxation, and cyclic tests. In simple tension, we observe that at lower

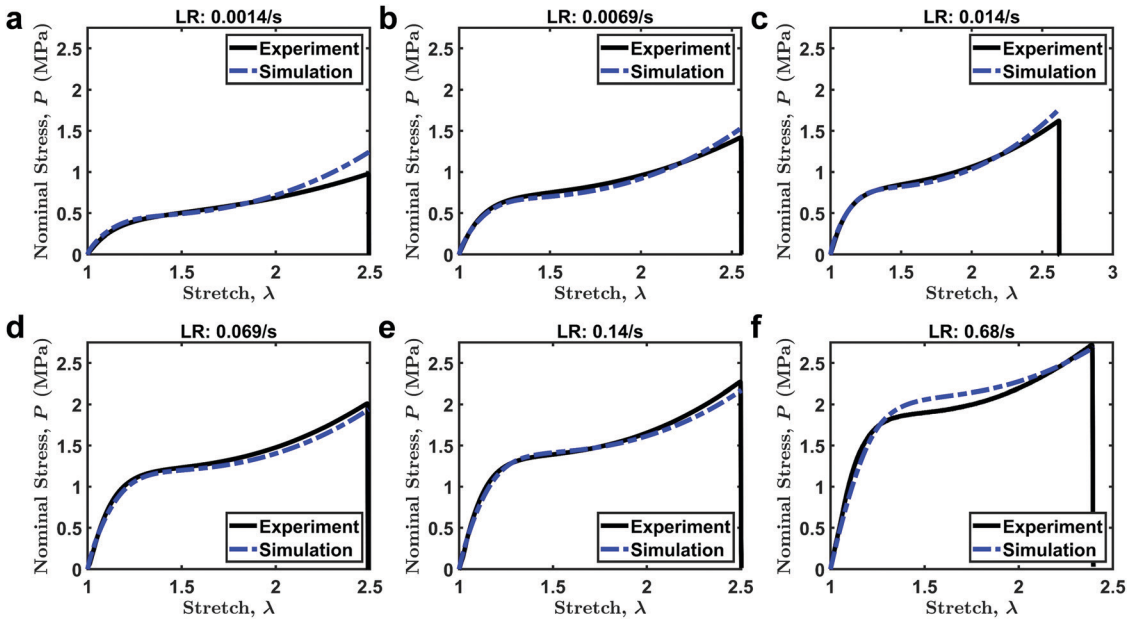


Fig. 4 Nominal stress $P$ (MPa) *vs.* stretch $\lambda$ for simple tension tests with six loading rates (LR) are presented here. (a) 0.0014 $s^{-1}$, (b) 0.0069 $s^{-1}$, (c) 0.014 $s^{-1}$, (d) 0.069 $s^{-1}$, (e) 0.14 $s^{-1}$, and (f) 0.68 $s^{-1}$. Solid black lines represent the experiment data and our simulation results using parameters in Table 1 are shown as dash-dotted blue lines.

 

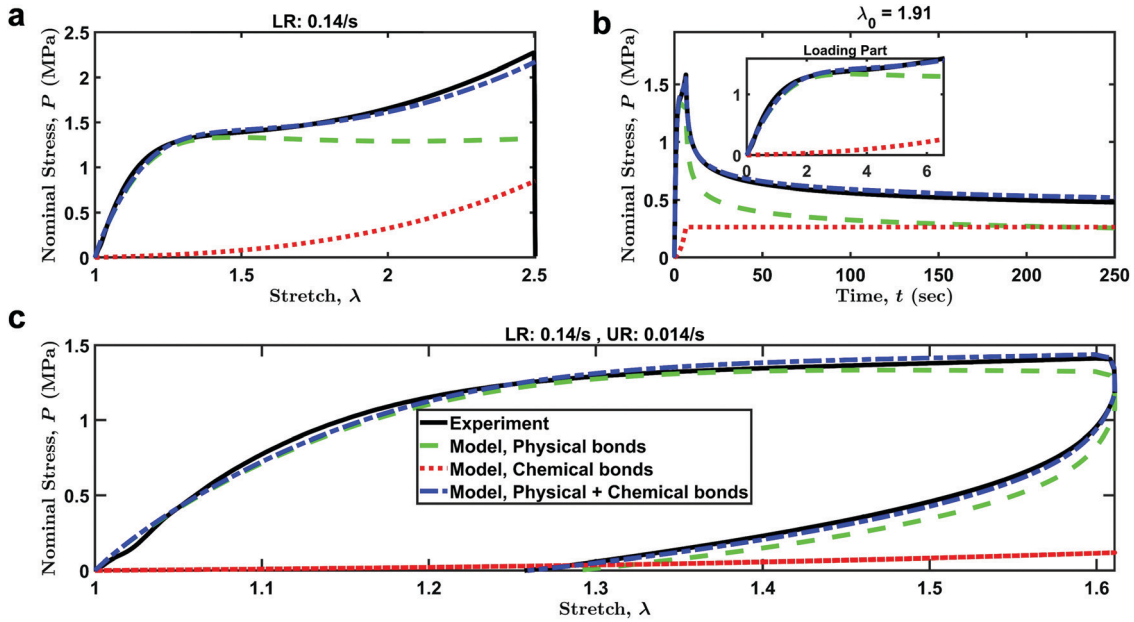


Fig. 5 For different loading histories, stress contributions from both physical and chemical bonds are computed using our model. (a) Simple tension, (b) tensile-relaxation, and (c) cyclic test. The tensile test is carried out using a loading rate (LR) of 0.14 $s^{-1}$. The stretch ratio in the tensile-relaxation test is $\lambda_0 \approx 1.91$. The cyclic test has a loading rate (LR) of 0.14 $s^{-1}$ and an unloading rate (UR) of 0.014 $s^{-1}$. Solid black lines represent the experiment data, the stress contribution from physical bonds is shown in green dotted lines, the stress contribution from chemical bonds is shown in red dotted lines, and total stress contribution from both physical and chemical bonds is represented by blue dash-dotted lines.

stretch ratios, most of the stress is carried by physical bonds. This is because $\omega_{chem} = 0.01$, so most of the load is carried by the physical crosslinks (recall $\rho \approx 0.97$ at the beginning of test, see Table 1). At higher stretch ratios ($>2.2$), due to accelerated breaking, a significant fraction of physical bonds break, so the chemical network starts to carry more load. In the tensile-relaxation test, most of the load is carried by physical bonds during the loading phase as the stretch ratios are too low to activate accelerated bond breaking. During relaxation, the healed bonds do not carry any load (the integral term in eqn (1a) is practically zero). As the initially connected physical bonds continue to break, the stress contribution from these bonds decreases continuously and the load is carried entirely by the chemical crosslinks. During the cyclic test, as the maximum strains are around 60%, most of the load is carried by physical bonds as the fraction of chemical bonds in the network is only 1%.

Next, we study the healing rate predicted by our model during these experiments.

Fig. 6 presents a few representative time dependent healing rates for simple tension, tensile-relaxation, and cyclic tests.

Fig. 6a shows that in a simple tension test, the healing rate first increases and then reaches a plateau. In the increasing region, the number of broken physical crosslinks increases, and since healing rate is proportional to the number of broken bonds, the healing rate increases too. At some point there is no further increase in the number of broken physical bonds, and the healing rate becomes approximately constant. Fig. 6b shows that during the relaxation part of a tensile-relaxation test, the reattached physical bonds do not carry load, and they break continuously. At long times, the load is carried entirely by the chemical network. In a cyclic test (Fig. 6c and d), the healing rate of physical bonds increases during the loading phase. During unloading, either there is a drop in the healing rate or there is hardly any increase after the peak of the loading phase. In Fig. 6c, the loading rate is much faster than the unloading rate, so the behavior is similar to the relaxation test, *i.e.*, the physical crosslinks that reattach during unloading carry very little load. This situation is different in Fig. 6d where the loading and unloading rates are similar, so the physical crosslinks that reattached after the peak load carry substantial load.

## 6. Discussion and conclusion

A finite strain constitutive model with time, rate, and strain dependent bond kinetics is used to study the viscoelastic behavior of the chemical PA gel. Our model predictions agree well with experimental behavior of the gel for simple tension, tensile-relaxation, and cyclic (loading–unloading) tests.

We found that the fitting is not sensitive to the choice of strain energy function. This is reasonable since the failure stretch of these chemical gels is around 2.5, so strain hardening effects are not expected to be significant. Data fitting is more sensitive to the choice of the accelerated breaking function $f$ in eqn (5). Here we note that the accelerated breaking function $f$ given by eqn (5) differs from our previous work[33] which is

$$f(I_1) = \exp\left\{\left(1 + \frac{I_1 - 3}{I_c - 3}\right)^m - 1\right\}, \quad I_c = \lambda_c^2 + \frac{2}{\lambda_c}. \qquad (7)$$

In the ESI† (Section S7), we show that our experiments can be fitted almost as well with this accelerated breaking function.

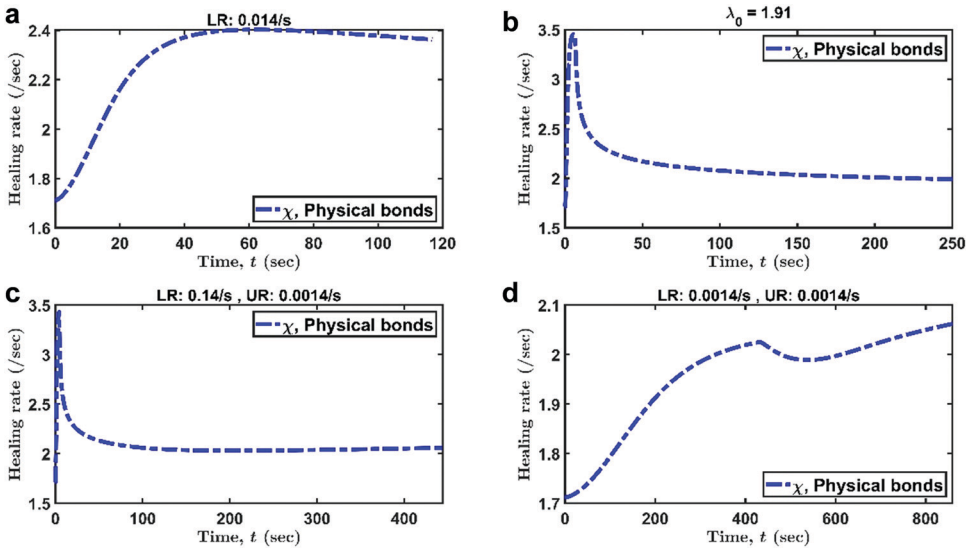


Fig. 6 Healing rate ($\chi(t)$) (in $s^{-1}$) for physical bonds (blue dash-dotted lines) *vs.* time (s) for three types of mechanical testing are shown here. (a) The top left plot is a simple tension test for a constant loading rate (LR) where $\dot{\lambda} = 0.014\ s^{-1}$. (b) The top right plot is a tensile-relaxation test with a stretch ratio of $\lambda_0 \approx 1.91$. (c and d) The two lower plots are cyclic tests with a loading–unloading rates (LR–UR) of 0.14–0.0014 $s^{-1}$ and 0.0014–0.0014 $s^{-1}$ respectively. The unloading starts at a strain of around 60%.

However, the critical stretch ratio $\lambda_c$ required to produce a good fit is around 1.08, which is lower than what we observe in our experiments ($\lambda_c \in (1.2, 1.3)$). The substantial differences in mechanical behavior of the two systems (chemical + physical *vs.* pure physical gel) suggested that the breaking kinetics of bonds in the two systems can be different. Because of this, we use the power law breaking accelerated function given by eqn (5).

In this paper, the behavior of the gel is studied only under uniaxial loading. We notice that in simple tension tests at very slow loading rates ($\sim 0.0014\ s^{-1}$), the stress is overestimated by our model. Our model requires more scrutiny in this regime. By subjecting the gel to multi-axial loading and more complex loading histories, we intend to address the limitations and improve our model in a future work.

## Conflicts of interest

We declare no conflicts of interest.

## Acknowledgements

This material is based on the work supported by the National Science Foundation under Grant No. CMMI-1903308. J. P. G. acknowledges support from the Japan Society for the Promotion of Science KAKENHI (grant no. JP17H06144). K. P. C. acknowledges support from the Japan Society for the Promotion of Science KAKENHI (grant no. JP19K23617). J. P. G. and K. P. C. acknowledge support from the Institute for Chemical Reaction Design and Discovery by World Premier International Research Initiative, MEXT, Japan.

## References

1 K. Y. Lee and D. J. Mooney, *Chem. Rev.*, 2001, **101**, 1869–1880.
2 B. R. Freedman and D. J. Mooney, *Adv. Mater.*, 2019, **31**, 1806695.
3 C. K. Kuo and P. X. Ma, *Biomaterials*, 2001, **22**(6), 511–521.
4 H. J. Kwon, *Adv. Mater. Sci. Eng.*, 2014, **2014**, 1–7.
5 H. J. Kwon, K. Yasuda, J. P. Gong and Y. Ohmiya, *Macromol. Res.*, 2014, **22**, 227–235.
6 T. I. Md. Mredha, Y. Z. Guo, T. Nonoyama, T. Nakajima, T. Kurokawa and J. P. Gong, *Adv. Mater.*, 2018, **30**, 1704937.
7 T. R. Hoare and D. S. Kohane, *Polymer*, 2008, **49**, 1993–2007.
8 Y. Qiu and K. Park, *Adv. Drug Delivery Rev.*, 2012, **64**, 49–60.
9 K. Park, W. S. W. Shalaby and H. Park, *Biodegradable hydrogels for drug delivery*, Technomic Pub, Lancaster, PA, 1993.
10 J. P. Gong, *Soft Matter*, 2010, **6**, 2583.
11 J. P. Gong, Y. Katsuyama, T. Kurokawa and Y. Osada, *Adv. Mater.*, 2003, **15**, 1155–1158.
12 Y.-H. Na, T. Kurokawa, Y. Katsuyama, H. Tsukeshiba, J. P. Gong, Y. Osada, S. Okabe, T. Karino and M. Shibayama, *Macromolecules*, 2004, **37**, 5370–5374.
13 A. Nakayama, A. Kakugo, J. P. Gong, Y. Osada, M. Takai, T. Erata and S. Kawano, *Adv. Funct. Mater.*, 2004, **14**, 1124–1128.
14 J. P. Gong, *Science*, 2014, **344**, 161–162.
15 J.-Y. Sun, X. Zhao, W. R. K. Illeperuma, O. Chaudhuri, K. H. Oh, D. J. Mooney, J. J. Vlassak and Z. Suo, *Nature*, 2012, **489**, 133–136.
16 T. Nakajima, H. Sato, Y. Zhao, S. Kawahara, T. Kurokawa, K. Sugahara and J. P. Gong, *Adv. Funct. Mater.*, 2012, **22**, 4426–4432.
17 Y. N. Ye, M. Frauenlob, L. Wang, M. Tsuda, T. L. Sun, K. Cui, R. Takahashi, H. J. Zhang, T. Nakajima, T. Nonoyama, T. Kurokawa, S. Tanaka and J. P. Gong, *Adv. Funct. Mater.*, 2018, **28**, 1801489.

 

18 Y. Huang, D. R. King, T. L. Sun, T. Nonoyama, T. Kurokawa, T. Nakajima and J. P. Gong, *Adv. Funct. Mater.*, 2017, **27**, 1605350.
19 H. Guo, C. Mussault, A. Brûlet, A. Marcellan, D. Hourdet and N. Sanson, *Macromolecules*, 2016, **49**, 4295–4306.
20 T.-T. Mai, T. Matsuda, T. Nakajima, J. P. Gong and K. Urayama, *Soft Matter*, 2019, **15**, 3719–3732.
21 C. Bilici, S. Ide and O. Okay, *Macromolecules*, 2017, **50**, 3647–3654.
22 R. Tamate, K. Hashimoto, T. Horii, M. Hirasawa, X. Li, M. Shibayama and M. Watanabe, *Adv. Mater.*, 2018, **30**, 1802792.
23 X. Hu, M. Vatankhah-Varnoosfaderani, J. Zhou, Q. Li and S. S. Sheiko, *Adv. Mater.*, 2015, **27**, 6899–6905.
24 H. J. Zhang, T. L. Sun, A. K. Zhang, Y. Ikura, T. Nakajima, T. Nonoyama, T. Kurokawa, O. Ito, H. Ishitobi and J. P. Gong, *Adv. Mater.*, 2016, **28**, 4884–4890.
25 T. L. Sun, T. Kurokawa, S. Kuroda, A. Bin Ihsan, T. Akasaki, K. Sato, M. A. Haque, T. Nakajima and J. P. Gong, *Nat. Mater.*, 2013, **12**, 932–937.
26 F. Luo, T. L. Sun, T. Nakajima, T. Kurokawa, Y. Zhao, K. Sato, A. B. Ihsan, X. Li, H. Guo and J. P. Gong, *Adv. Mater.*, 2015, **27**, 2722–2727.
27 X. Zhang, Y. Liu, J. Wen, Z. Zhao, H. Chen, X. Liu and S. Liu, *Soft Matter*, 2020, **16**, 3416–3424.
28 M. Nakahata, Y. Takashima and A. Harada, *Macromol. Rapid Commun.*, 2016, **37**, 86–92.
29 S. Burattini, H. M. Colquhoun, J. D. Fox, D. Friedmann, B. W. Greenland, P. J. F. Harris, W. Hayes, M. E. Mackay and S. J. Rowan, *Chem. Commun.*, 2009, 6717.
30 M. A. Haque, T. Kurokawa, G. Kamita and J. P. Gong, *Macromolecules*, 2011, **44**, 8916–8924.
31 D. C. Tuncaboylu, M. Sari, W. Oppermann and O. Okay, *Macromolecules*, 2011, **44**, 4997–5005.
32 R. Long, K. Mayumi, C. Creton, T. Narita and C.-Y. Hui, *Macromolecules*, 2014, **47**, 7243–7250.
33 S. P. Venkata, K. Cui, J. Guo, A. T. Zehnder, J. P. Gong and C.-Y. Hui, *Extreme Mech. Lett.*, 2021, **43**, 101184.
34 K. Cui, T. L. Sun, T. Kurokawa, T. Nakajima, T. Nonoyama, L. Chen and J. P. Gong, *Soft Matter*, 2016, **12**, 8833–8840.
35 K. Cui, T. L. Sun, X. Liang, K. Nakajima, Y. N. Ye, L. Chen, T. Kurokawa and J. P. Gong, *Phys. Rev. Lett.*, 2018, **121**, 185501.
36 X. Li, K. Cui, T. L. Sun, L. Meng, C. Yu, L. Li, C. Creton, T. Kurokawa and J. P. Gong, *Proc. Natl. Acad. Sci. U. S. A.*, 2020, **117**, 7606–7612.
37 T. L. Sun, F. Luo, W. Hong, K. Cui, Y. Huang, H. J. Zhang, D. R. King, T. Kurokawa, T. Nakajima and J. P. Gong, *Macromolecules*, 2017, **50**, 2923–2931.
38 K. Cui, Y. N. Ye, T. L. Sun, L. Chen, X. Li, T. Kurokawa, T. Nakajima, T. Nonoyama and J. P. Gong, *Macromolecules*, 2019, **52**, 7369–7378.
39 K. Cui, Y. N. Ye, T. L. Sun, C. Yu, X. Li, T. Kurokawa and J. P. Gong, *Macromolecules*, 2020, **53**, 5116–5126.
40 K. Cui, Y. N. Ye, C. Yu, X. Li, T. Kurokawa and J. P. Gong, *ACS Macro Lett.*, 2020, 1582–1589.
41 R. Long, K. Mayumi, C. Creton, T. Narita and C.-Y. Hui, *J. Rheol.*, 2015, **59**, 643–665.
42 J. Guo, R. Long, K. Mayumi and C.-Y. Hui, *Macromolecules*, 2016, **49**, 3497–3507.